Ab Initio Investigation of Electron Detachment in Dicarboxylate Dianions

John M. Herbert[†] and J. V. Ortiz*

Department of Chemistry, Kansas State University, Manhattan, Kansas 66506-3701

Received: July 26, 2000; In Final Form: September 26, 2000

Optimized structures for oxalate (C_2O_4), malonate ($O_2CCH_2CO_2$), and succinate ($O_2C(CH_2)_2CO_2$) mono- and dianions are computed at the level of second-order Møller−Plesset perturbation theory (MP2). For oxalate, both anions exhibit D_{2d} and D_{2h} rotamers, and in addition, for the singly charged species, we find an anion−molecule complex of the form $CO_2^-\cdot CO_2$. For the malonate and succinate anions we examine both keto and enol isomers; the keto structures are characterized by unhindered rotation of the CO_2 moieties about geometries of C_2 symmetry, while the enol isomers are much more rigid as a result of an intramolecular hydrogen bond. In both malonate and succinate, the enol isomer is the more stable form of the monoanion, while the keto isomer is the more stable dianion, although for $O_2CCH_2CO_2^{2-}$ the estimated isomerization barrier is only about 7 kcal/mol. All of the dianions are adiabatically unbound and the enol dianions are vertically unbound as well. However, vertical detachment energies calculated by electron propagator methods at the partial third-order (P3) quasiparticle level with large, highly polarized basis sets suggest that the more stable keto forms of $O_2CCH_2CO_2^{2-}$ and $O_2C(CH_2)_2CO_2^{2-}$ are metastable, with vertical detachment barriers of about 0.2 and 0.6 eV, respectively. These results complement recent experimental observations of small dicarboxylate dianions in the gas phase.

Introduction

The existence of multiply charged anions in the gas phase has been the subject of considerable experimental and theoretical investigation for several decades.[1−8] Much effort has been devoted to elucidation of the smallest molecular systems capable of forming stable, gas-phase polyanions. Equally interesting are the changes in electronic structure and molecular geometry that ensue when the polyanion X^{n-} ejects an electron to form $X^{(n-1)-}$. These changes ultimately dictate whether such an electron detachment process is spontaneous and hence whether X^{n-} is a stable anion.

Although not the smallest molecules known to support multiple negative charges, the unbranched dicarboxylate homologues $O_2C(CH_2)_nCO_2^{2-}$ are interesting targets for synthesis and theory. For $n = 3-7$, these dianions have been created in the gas phase via collisionally induced ion pair formation from singly-charged carboxylic esters,[4] and there is some circumstantial evidence for the existence of the $n = 2$ homologue as well.[9] Recently, Wang and co-workers[5] have produced dicarboxylate dianions with $n = 3-10$ using electrospray ionization, and in a similar fashion have created the $n = 2$ homologue (succinate) as a complex with a single water molecule.[6]

Electrospray ionization coupled with photoelectron spectroscopy[7] reveals that the $O_2C(CH_2)_nCO_2^{2-}$ anion is stable with respect to electron detachment when $n \geq 3$.[5,6] When $n = 2$ (and in the absence of any solvating water molecule), the dianion produces a weak signal in the mass spectrum,[5] but no electron binding energy has been measured, leading the researchers to conclude that bare $O_2C(CH_2)_2CO_2^{2-}$ is metastable, with a lifetime less than 0.1 s, and is bound only by a Coulomb barrier to the reaction $X^{2-} \rightarrow X^- + e^-$. For anions, such a barrier to electron detachment exists due to the high energetic cost of producing two negatively charged species in close proximity. For $n \leq 3$, Wang and co-workers[5] estimate this Coulomb barrier to be greater than 2.5 eV.

Previous Studies

Several authors have published Hartree−Fock (HF)-optimized structures and energies for a handful of symmetry-constrained conformers of $C_2O_4^-$ [10,11] and $C_2O_4^{2-}$,[11−14] and in addition Fleischman and Jordan[10] have perfomed MP2/6-31+G* single-point energy calculations on $C_2O_4^-$ structures optimized at the HF/6-31+G* level. For the closed-shell dianion, HF theory alone predicts a D_{2d} structure to be the most stable conformer. A D_{2h} rotamer lies an estimated 2−4 kcal/mol (0.1−0.2 eV) higher in energy.[13] However, HF calculations for the monoanion predict the most stable isomer to be a planar $CO_2^-\cdot CO_2$ complex in which the unpaired electron is localized on a single CO2 group. When Fleischman and Jordan[10] include correlation via a MP2/6-31+G*//HF/6-31+G* calculation, the planar $CO_2^-\cdot CO_2$ complex is a local minimum lying 5 kcal/mol (0.2 eV) above a D_{2d} minimum.

For malonate and larger dicarboxylates, a priori restriction to high-symmetry geometries is much more perilous and clearly an expanded search of configuration space is warranted. The torsional potential of $O_2CCH_2CO_2^{2-}$ has been studied at the HF/STO-3G level[15] with initial bond lengths and angles taken from crystallographic data.[16] Full HF optimization of this dianion has been carried out by Kang and co-workers[17] as well as by Deerfield and Pedersen.[18] The former obtain a HF/6-31+G**-optimized structure that is qualitatively similar to our MP2 -optimized structure of C_2 symmetry, although we shall argue below that this symmetry is not rigid because the CO2 groups rotate freely. Harmonic frequency calculations at the HF level confirm[18] that Deerfield and Pedersen's structure is indeed a local minimum.

Using HF/6-31++G** optimization, Deerfield and Pedersen[18] locate a second minimum for the malonate dianion,

* Corresponding author. E-mail ortiz@ksu.edu.
[†] Present address: Department of Chemistry, University of Wisconsin, 1101 University Ave., Madison, WI 53706.

10.1021/jp002657c CCC: $19.00
Published on Web 11/28/2000

corresponding to the enol structure $[O_2CCH{=}CO_2H]^{2-}$. MP2/6-31++G** single points carried out by these authors place the enol 31 kcal/mol above their minimum-energy C_2 O_2CCH_2-CO_2^{2-} keto structure, which is somewhat larger than the isomerization barrier that we calculate at the MP2 level.

Finally, Skurski et al.[19] have recently reported MP2-optimized structures for the succinate mono- and dianions. Up to rotation of the carboxylate groups, their optimized structures are essentially the same as ours, although their vertical detachment energies (calculated as the difference in CCSD(T) single points at the mono- and dianion MP2-optimized geometries) are about 0.2 eV less than our P3 values.

The structure of the malonate monoanion and the stability of free $O_2CCH_2CO_2^{2-}$ with respect to electron detachment have not been explored previously.

Computational Methods

Geometry optimizations were performed with Gaussian 98[20] using second-order Møller−Plesset perturbation theory (MP2)[21] and employing the 6-31+G*, 6-311+G*, and 6-311++G** basis sets.[22] Except where indicated, the default convergence criteria were used. For the open-shell monoanions, all optimized structures had $\langle S^2\rangle_{UHF} \leq 0.800$ prior to annihilation of the first spin contaminant.

Where computationally feasible, we have evaluated and reported (harmonic) vibrational frequencies at each optimized geometry. This includes all structures of oxalate and malonate except $O_2CCH_2CO_2^-$ at the MP2/6-311++G** level, where the basis size (168 functions) outstrips our ability to perform MP2 frequency calculations for an open-shell system. For succinate, frequencies are reported only for the dianion at the MP2/6-31+G* level.

We calculate vertical electron detachment energies (VEDEs) and adiabatic electron detachment energies (AEDEs) in two ways. The conceptually simple approach is to use the definitions[2]

$$\mathrm{VEDE} = E^{(1-)}(\vec{r}_e^{\,(2-)}) - E^{(2-)}(\vec{r}_e^{\,(2-)})$$

$$\mathrm{AEDE} = E^{(1-)}(\vec{r}_e^{\,(1-)}) - E^{(2-)}(\vec{r}_e^{\,(2-)})$$

where $E^{(1-)}$ and $E^{(2-)}$ represent the mono- and dianion energies, respectively, while $\vec{r}_e^{(1-)}$ and $\vec{r}_e^{(2-)}$ denote their respective minimum-energy geometries. These energies are each calculated at the MP2 level and we refer to this as the ΔMP2 method. In cases where harmonic frequencies have been computed, we can similarly compute the zero-point-corrected AEDE, $AEDE_0$, by substituting zero-point corrected energies for $E^{(1-)}$ and $E^{(2-)}$.

In calculating VEDEs by ΔMP2, it is often the case that the unrestricted HF wave function for the monoanion, calculated at the optimized geometry of the dianion, suffers from pronounced spin contamination. In our tabulations, we indicate all cases in which $\langle S^2\rangle_{UHF} \geq 0.800$ (see Tables 14 and 21 in which we tabulate VEDEs for malonate and succinate). $\langle S^2\rangle_{UHF}$ values for each *optimized* monoanion structure are reported in Table 1 and are free of significant spin contamination.

In addition to the ΔMP2 technique, we calculate VEDEs using electron propagator methods,[3] subject to the partial third-order (P3) quasiparticle approximation.[24] This method achieves more accurate orderings of electronic states than HF calculations, while preserving the HF orbital interpretation that is often lost in the ΔMP2 and similar correlated, perturbative comparisons of initial and final state energies. In addition to the aforementioned basis sets exploited for MP2 calculations, our P3 calculations employ the highly polarized 6-311++G(2df,p) and 6-311++G(2df,2pd) bases[22,25] as well several highly diffuse basis sets. The latter are indicated by a "+++" designation, where, for example, the 6-311+++G** basis consists of the standard 6-311++G** basis augmented with an additional set of valence *s*- and *sp*-type functions on the heavy atoms; the orbital exponents of these additional diffuse functions are one-third those of the exponents in the first set of diffuse valence functions.

For each P3 calculation, we report all negative detachment energies (indicating unbound electrons). When all vertical detachment energies are positive we report only the smallest value. Each reported P3 detachment energy corresponds to a pole strength greater than 0.89.

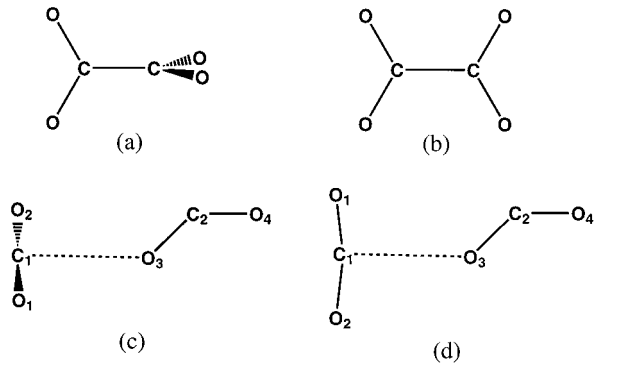

Figure 1. Optimized structures of oxalate anions: (a) D_{2d} potential minimum of $C_2O_4^-$ and $C_2O_4^{2-}$; (b) planar D_{2h} transition state of $C_2O_4^-$ and $C_2O_4^{2-}$; (c) nonplanar C_s minimum of $C_2O_4^-$; (d) planar C_s transition state of $C_2O_4^-$. HF/6-31+G*, MP2/6-31+G*, and MP2/6-311+G* optimizations each yield qualitatively similar structures.

TABLE 1: $\langle S^2\rangle$ Values for the UHF Reference Wave Functions of MP2-Optimized Monoanion Structures

monoanion		optimized $\langle S^2\rangle_{UHF}$ 6-31+G*	optimized $\langle S^2\rangle_{UHF}$ 6-311++G**
oxalate	D_{2d}	0.7709	0.7690
	D_{2h}	0.7605	0.7605
	planar C_s	0.7615	0.7616
	nonplanar C_s	0.7620	0.7615
malonate	C_1 keto	0.7586	0.7584
	C_2 keto	0.8001	0.7989
	C_s keto	0.7590	0.7587
	C_s enol	0.7947	0.7902
succinate	C_2 keto	0.7804	0.7804
	C_i keto	0.7804	0.7804
	C_1 enol	0.7858	0.7835

Results and Discussion

Oxalate. For the oxalate dianion, optimization reveals two rotamers: a D_{2d} potential minimum and a D_{2h} transition state (Figure 1). Rotation about and slight lengthening of the C−C bond convert the minimum into the transition state, which at the MP2/6-311+G* level lies 0.24 eV above the minimum and has an imaginary frequency of $84.5i$ cm^{-1} for a mode that is essentially rotation about the C−C axis. Table 2 compares geometry data optimized at the MP2/6-31+G* level to those optimized at the MP2/6-311+G* level. Addition of a third set of valence orbitals produces minimal change in bond angles and also very little change (<0.01 Å) in the bond lengths of either conformer.

Optimization of the simple anion $C_2O_4^-$ also produced a D_{2d} minimum and a D_{2h} transition state like those in Figure 1, but with a smaller rotation barrier separating the two conformers (0.08 eV at the MP2/6-311+G* level). An imaginary frequency

TABLE 2: MP2-Optimized Parameters for $C_2O_4^{2-}$ and $C_2O_4^-$ [a]

basis set	point group	E	O−C−O angle, deg	bond lengths, Å C−O	bond lengths, Å C−C
$C_2O_4^{2-}$					
6-31+G*	D_{2d}	−376.158 76[b]	126.4	1.279	1.554
	D_{2h}	0.27[c]	126.0	1.276	1.615
6-311+G*	D_{2d}	−376.412 35[b]	126.5	1.270	1.558
	D_{2h}	0.24[c]	126.2	1.267	1.621
$C_2O_4^-$					
6-31+G*	D_{2d}	−376.246 99[b]	142.4	1.230	1.858
	D_{2h}	0.12[c]	146.1	1.221	2.189
6-311+G*	D_{2d}	−376.507 15[b]	143.1	1.219	1.895
	D_{2h}	0.08[c]	146.6	1.210	2.200

[a] In each case, the D_{2d} structure is a local minimum and the D_{2h} geometry is a transition state. [b] MP2 energy in atomic units. [c] MP2 energy relative to the corresponding D_{2d} minimum, in electronvolts.

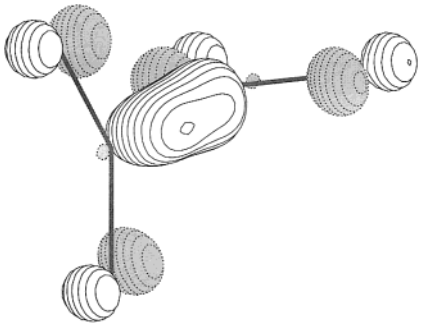

Figure 2. Highest occupied molecular orbital of $^2A_1$ $C_2O_4^-$, as obtained at the MP2/6-311+G* geometry.

of 36.7 cm^{-1} corresponds once again to stretching of and rotation about the C−C bond. We thus conclude that D_{2h}−D_{2d} interconversion is facile in $C_2O_4^-$. As with the dianion, addition of a third set of valence functions to the basis does not significantly alter bond angles in $C_2O_4^-$, although the 0.04 Å increase in C−C bond length is somewhat greater than the corresponding increase in the dianion.

Figure 2 presents a contour plot of the highest occupied molecular orbital (HOMO) of $^2A_1$ $C_2O_4^-$. This orbital, which resembles qualitatively the HOMO of the dianion, is delocalized over the entire oxalate molecule. It is bonding with respect to the C−C interaction and antibonding with respect to each C−O interaction, which explains why the C−C bond length increases and the C−O lengths decrease when $C_2O_4^{2-}$ ejects an electron and relaxes to the optimum geometry of the monoanion.

In addition to D_{2d} and D_{2h} structures, we locate a second minimum for $C_2O_4^-$ at the C_s geometry depicted in Figure 1c, in which the two CO_2 moieties lie in perpendicular planes. An essentially rigid rotation of one CO_2 moiety produces the planar C_s transition state of Figure 1d; the planar geometry has an imaginary out-of-plane bending mode of 45.6i cm^{-1}. Interconversion of the two C_s conformers is unhindered (<0.001 eV barrier) and preserves the bond lengths and angles within the individual CO_2 moieties.

Optimized parameters for the C_s configurations of $C_2O_4^-$ are listed in Table 3. Note in particular the large (2.6 Å) distance between CO_2 moieties, indicative of an anion−molecule complex. Furthermore, in both C_s conformers the unpaired electron in the HOMO is localized entirely on the more bent CO_2 group. This fact, coupled with the near-linearity of the other carboxylate group, suggests that the two C_s structures are best described as CO_2^- solvated by a (neutral) carbon dioxide molecule. (For comparison, at the MP2/6-311+G* level, free CO_2 has bond lengths of 1.169 Å, while the CO_2^- anion has bond lengths of 1.236 Å and a bond angle of 134.7°.) By comparison of the relative energies of the optimized oxalate structures (Table 4), we see that the C_s minimum of $C_2O_4^-$ is higher in energy than even the D_{2h} transition state of this anion, which further suggests that the C_s structures represent merely the van der Waals minimum in the dissociation pathway $C_2O_4^- \rightarrow CO_2 + CO_2^-$.

TABLE 3: MP2-Optimized Bond Lengths and Angles for C_s Isomers of $CO_2^-\cdot CO_2$[a] Atom labels refer to Figure 1c,d

basis set	bond lengths, Å C_1-O_1	C_1-O_3	O_3-C_2	C_2-O_4	bond angles, deg $O_1C_1O_2$	$C_1O_3C_2$	$O_3C_2O_4$
Nonplanar C_s Minimum							
6-31+G*	1.181	2.600	1.253	1.244	172.1	109.5	136.1
6-311+G*	1.170	2.636	1.242	1.233	172.9	109.3	136.9
Planar C_s Transition State							
6-31+G*	1.181	2.582	1.254	1.244	172.4	130.8	135.7
6-311+G*	1.170	2.614	1.242	1.234	173.2	132.4	136.4

[a] In the nonplanar geometry, the $O_1-C_1-O_2-O_3$ dihedral angle is 172.9° at the MP2/6-311+G* Level.

TABLE 4: Relative Energies of $C_2O_4^-$ and $C_2O_4^{2-}$ Isomers at the MP2/6-311+G* Level

structure		classification	E
$C_2O_4^{2-}$	D_{2d}	local minimum	−376.412 35[a]
	D_{2h}	transition state	0.24[b]
$C_2O_4^-$	D_{2d}	local minimum	−376.507 15[a]
	D_{2h}	transition state	0.08[c]
	C_s	local minimum	0.23[c]
	C_s	transition state	0.25[c]
$CO_2 + CO_2^-$		complete dissociation	0.53[c]

[a] MP2/6-311+G* energy (atomic units). [b] Energy (eV) relative to the D_{2d} minimum of $C_2O_4^{2-}$. [c] Energy (eV) relative to the D_{2d} minimum of $C_2O_4^-$.

TABLE 5: ΔMP2 Electron Detachment Energies (eV) for $C_2O_4^{2-}$ [a]

basis set	ΔMP2 VEDE	ΔMP2 AEDE	ΔMP2 $AEDE_0$
MP2/6-31+G* Geometry			
6-31+G*	−1.62	−2.40	−2.42
6-311+G*	−1.66	−2.57	
6-311+G(2df)	−1.50	−2.42	
6-311+++G*	−1.20	−2.10	
MP2/6-311+G* Geometry			
6-311+G*	−1.74	−2.58	−2.60
6-311+G(2df)	−1.57	−2.43	
6-311+++G*	−1.28	−2.11	

[a] The "+ + +" designation indicates additional heavy-atom diffuse functions.

Because of the nontrivial C−C rotation barrier in the oxalate dianion, we calculate VEDEs only from the minimum-energy D_{2d} geometry. ΔMP2 detachment energies (both vertical and adiabatic) for D_{2d} $C_2O_4^{2-}$ are listed in Table 5, while P3 VEDEs using several large basis sets are reported in Table 6. A negative detachment energy implies that the dianion is unbound, and with the smaller basis sets several electrons are unbound at the P3 level. In each case, however, the most negative detachment energy belongs to the a_1 HOMO. (The ΔMP2 calculations always correspond to detachment from the HOMO.) The ΔMP2 vertical detachment energies tend to be about 0.55 eV more negative than the P3 values except for the 6-311+++G* basis, where both methods yield approximately the same value.

Malonate. Structures of $O_2CCH_2CO_2^{2-}$ and $O_2CCH_2CO_2^-$. Optimization of $O_2CCH_2CO_2^{2-}$ resulted in structures a, b, and d of Figure 3, with relative energies tabulated in Table 7. Two

TABLE 6: P3 Vertical Detachment Energies (eV) for $C_2O_4^{2-}$ [a]

	geometry	
P3 basis set	6-31+G*	6-311+G*
6-311+G*	−1.08 (a_1)	−1.18 (a_1)
	−0.12 (e)	−0.15 (e)
	−0.06 (a_2)	−0.08 (a_2)
6-311+G(2df)	−0.93 (a_1)	−1.02 (a_1)
6-311+G(3d2f)	−0.88 (a_1)	−0.97 (a_1)
6-311+++G*	−1.16 (a_1)	−1.25 (a_1)
	−0.16 (a_2)	−0.19 (a_2)
	−0.06 (e)	−0.09 (e)
6-311+++G(2df)	−0.88 (a_1)	−0.97 (a_1)
6-311+++G(3d2f)	−0.83 (a_1)	−0.93 (a_1)

[a] All orbitals found to contain unbound electrons are listed, by symmetry; the a_1 orbital is the HOMO. The "+ + +" bases contain extra diffuse functions.

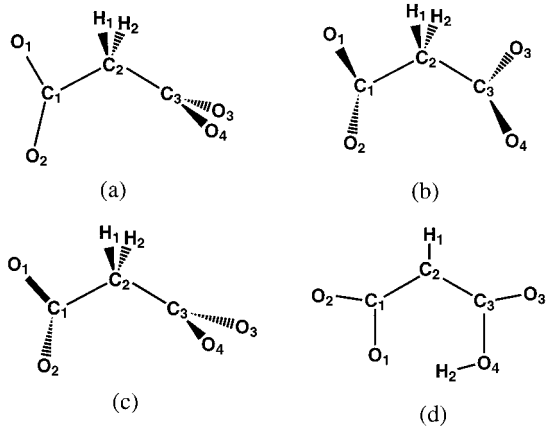

Figure 3. Optimized keto and enol structures for malonate anions: (a) C_s (keto) configuration; (b) C_2(keto) configuration; (c) C_1(keto) configuration; (d) planar C_s (enol) configuration. $O_2CCH_2CO_2^-$ exhibits all four structures as minima or transition states; the dianion exhibits all but c.

TABLE 7: MP2 Energies and Lowest Vibrational Frequencies of Optimized Malonate Structures

basis set	conformer	E	low freq., cm^{-1}
$O_2CCH_2CO_2^{2-}$			
6-31+G*	C_s(keto)	−415.347 63[a]	8.7 (A'')
	C_2(keto)	0.00[b]	15.5i (B)[c]
	C_s(enol)	0.63[b]	92.5 (A'')
6-311++G**	C_2(keto)	−415.644 82[a]	25.7 (B)
	C_s(keto)	0.00[b]	14.9i (A'')[c]
	C_s(enol)	0.45[b]	54.3 (A'')
$O_2CCH_2CO_2^-$			
6-31+G*	C_s(enol)	−415.405 00[a]	84.4 (A'')
	C_2(keto)	0.71[b]	17.5i (B)[c]
	C_1(keto)	1.34[b]	33.8 (A)
	C_s(keto)	1.52[b]	64.6i (A'')
6-311++G**	C_s(enol)	−415.709 37[a]	
	C_2(keto)	0.81[b]	
	C_1(keto)	1.48[b]	
	C_s(keto)	1.66[b]	

[a] MP2 energy in atomic units. [b] Energy (eV) relative to the lowest-energy structure at the same level of theory. [c] Tight convergence criteria were employed in these optimizations.

of the structures are conformers of the keto isomer, while the third is the structurally dissimilar enol isomer created (formally) by protonation of an oxygen atom and formation of a C−C double bond. Harmonic frequency calculations establish the enol structure and one keto conformer as local minima, while the other keto conformer is a transition state. However, which keto structure exhibits the imaginary frequency depends on the level

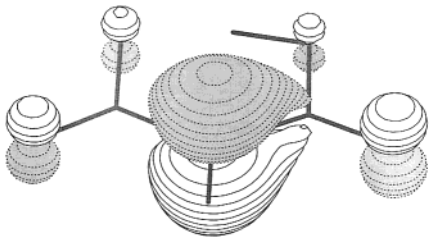

Figure 4. Highest occupied molecular orbital of the enol isomer of $^1A'$ $O_2CCH_2CO_2^{2-}$, obtained at the MP2/6-311++G** geometry.

TABLE 8: MP2-Optimized Geometry Data for the C_2 Conformer of Keto Malonate[a]

	bond lengths, Å			angles, deg		
basis set	C_1-C_2	C_1-O_1	C_1-O_2	$O_1C_1O_2$	$C_1C_2C_3$	$O_1C_1C_2H_1$
$O_2CCH_2CO_2^{2-}$						
6-31+G*	1.551	1.282	1.272	126.5	119.0	6.9
6-311++G**	1.556	1.271	1.263	126.9	118.9	5.2
$O_2CCH_2CO_2^-$						
6-31+G*	1.592	1.266	1.234	135.1	109.7	19.6
6-311++G**	1.598	1.256	1.224	135.5	109.6	19.3

[a] Atom labels correspond to Figure 3b.

of theory. At the HF/6-31+G* level, the C_2(keto) structure is the potential minimum and the C_s(keto) structure is a transition state. At the MP2/6-31+G* level the opposite is observed, but upon extension of the basis to 6-311++G**, MP2 optimization once again reveals a C_2 minimum and a C_s transition state. Jordan[10,11] observes similar basis set effects in $C_2O_4^-$ that change the order of the energies of the D_{2h}, D_{2d}, and C_s structures and also cause minima and transition states to exchange roles depending upon which basis set is used (Figure 4).

Some optimized structural parameters for the C_2(keto) conformer of malonate are listed in Table 8, while Table 9 provides geometry data for the C_s(keto) conformer. As with oxalate, changes in bond lengths beyond the MP2/6-31+G* level are on the order of 0.01 Å and changes in bond angles are one degree or less, with the exception of the $O_1-C_1-C_2-H_1$ dihedral angle of the dianion. There is considerable freedom in this coordinate, as we now discuss.

The frequency and symmetry of the lowest vibrational mode of each $O_2CCH_2CO_2^{2-}$ optimized structure are listed in Table 7. For both keto isomers, the lowest mode interconverts the C_s and C_2 structures via rotation of the two CO_2 moieties in opposite directions about the two C−C bond axes. The frequencies (real or imaginary) associated with these modes are small, so the carboxylate groups undergo large amplitude rotations about the C−C bonds. Moreover, the calculated energy difference between the two keto conformers is negligible and we conclude that the carboxylate groups *in the keto isomer* rotate freely in the gas phase.

In contrast, the enol isomer is not characterized by such free rotation: the smallest vibrational frequency of the C_s (enol) structure is a CH wag of 54.3 cm^{-1}. The rigidity of this structure is the pale shadow of an intramolecular hydrogen bond, as evidenced by the relatively short (1.495 Å) O_1-H_2 distance (Tables 10 and 11). Our optimized MP2/6-311++G** structures for keto and enol $O_2CCH_2CO_2^{2-}$ put the enol isomer 0.45 eV (10 kcal/mol) above the minimum-energy C_2 (keto) structure. However, at the MP2/6-311++G(2df,2pd)//MP2/6-311++G** level this isomerization barrier is a more modest 0.29 eV (7 kcal/mol), so that while the keto isomer should dominate the gas-phase dynamics of this dianion, one cannot completely ignore the enol variety.

TABLE 9: MP2-Optimized Bond Lengths and Angles for the C_s Conformer of Keto Malonate[a]

	bond lengths, Å					angles, deg		
basis set	C_1-O_1	C_1-O_2	C_3-O_3	C_1-C_2	C_2-C_3	$O_1C_1O_2$	$C_1C_2C_3$	$O_3C_3O_4$
$O_2CCH_2CO_2^{2-}$								
6-31+G*	1.285	1.264	1.278	1.561	1.542	126.8	120.3	126.4
6-311++G**	1.275	1.255	1.269	1.567	1.546	127.3	120.6	126.8
$O_2CCH_2CO_2^-$								
6-31+G*	1.356	1.220	1.261	1.502	1.575	119.1	112.0	131.4
6-311++G**	1.346	1.211	1.250	1.505	1.583	119.7	111.9	132.0

[a] Atom labels refer to Figure 3a.

TABLE 10: MP2-Optimized Bond Lengths for the Planar Enol Structure of Malonate[a]

	bond lengths, Å							
basis set	C_1-O_1	C_1-O_2	C_1-C_2	C_2-C_3	C_3-O_3	C_3-O_4	O_4-H_2	O_1-H_2
$O_2CCH_2CO_2^{2-}$								
6-31+G*	1.316	1.284	1.466	1.412	1.273	1.392	1.028	1.585
6-311++G**	1.310	1.273	1.466	1.417	1.263	1.379	1.031	1.495
$O_2CCH_2CO_2^-$								
6-31+G*	1.291	1.255	1.503	1.485	1.232	1.332	1.049	1.510
6-311++G**	1.287	1.242	1.504	1.489	1.226	1.319	1.069	1.392

[a] Atom labels refer to Figure 3d.

TABLE 11: MP2-Optimized Bond Angles for the Planar Enol Structure of Malonate[a]

	angles, deg					
basis set	$O_1-C_1-O_2$	$O_1-C_1-C_2$	$C_1-C_2-C_3$	$C_2-C_3-O_4$	$O_3-C_3-O_4$	$C_3-O_4-H_2$
$O_2CCH_2CO_2^{2-}$						
6-31+G*	122.4	118.1	125.9	116.3	116.5	102.6
6-311++G**	122.6	117.2	124.9	115.4	117.5	101.7
$O_2CCH_2CO_2^-$						
6-31+G*	127.8	115.2	124.5	114.8	122.3	104.9
6-311++G**	127.8	114.3	123.2	113.8	124.2	103.5

[a] Atom labels refer to Figure 3d.

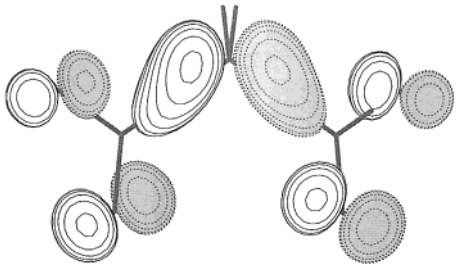

Figure 5. Highest occupied molecular orbital of ^2B $O_2CCH_2CO_2^-$, obtained at the MP2/6-311++G** geometry.

While the keto isomer of $O_2CCH_2CO_2^{2-}$ is somewhat more stable than the enol form, for the singly charged species the enol isomer, Figure 3d, is more stable. In addition to an enol potential minimum for $O_2CCH_2CO_2^-$, at the MP2/6-31+G* level we obtain optimized C_2(keto), C_s(keto), and C_s(enol) structures that are qualitatively similar to the corresponding dianion structures except that for the monoanion both the C_s and C_2 keto structures exhibit a single imaginary frequency. At this level, only the C_1 conformer of Figure 3a is found to be a rigorous potential minimum. This structure is obtained from the C_s transition state via rotation of the carboxylate group that lies in the mirror plane, followed by elongation of one C−O bond in the other carboxylate group. The C_1 minimum thus obtained lies a mere 0.18 eV (4 kcal/mol) below the C_s transition state, consistent with the low-frequency (33.8 cm^{-1}) carboxylate rotation at the C_1 minimum. This rotation tends to interconvert the C_s and C_1 keto structures.

In Figure 5 we present a contour plot of the HOMO of ^2B $O_2CCH_2CO_2^-$ (keto isomer); the HOMO of the dianion bears the same qualitative features, namely, constructive interference along the C−C bonds and nodes along each C−O bond. As with oxalate, this explains why the monoanion has longer C−C bond lengths and shorter C−O bond lengths than the dianion.

While we accept that the C_s(keto) conformation of $O_2CCH_2CO_2^-$ is a *bona fide* saddle point on the potential surface, we contend that the C_2 conformation (whose energy is significantly lower than other optimized keto structures for the malonate monoanion) is actually a potential minimum, and that the imaginary frequency of 17.5i cm^{-1} obtained at the MP2/6-31+G* level with tight convergence criteria is erroneous. As evidence, we performed MP2/6-31+G* single-point calculations on the simple anion for geometries distorted from C_2 by a small scalar multiple λ of the normal mode eigenvector corresponding to the imaginary frequency. The step sizes and energies relative to the C_2 geometry are listed in Table 12.

Note from Table 12 that energy increases in both directions along the normal mode eigenvector, indicating that at the C_2 geometry ($\lambda = 0$) the harmonic force constant $\partial^2E/\partial\lambda^2$ should be positive. Furthermore, polynomial fits of $E(\lambda)$ about $\lambda = 0$ require higher-order derivatives, with magnitudes comparable to or greater than $|\partial^2E/\partial\lambda^2|$, to produce an accurate fit over the entire range of step sizes in Table 12. Thus, even for vibrational displacements on the order of 0.01 Å or less, the harmonic picture is inadequate. If, however, one restricts attention to a smaller radius around $\lambda = 0$, say, by discarding the last four data points in Table 12, then a quadratic fit suffices, and one obtains a value of 150 cm^{-1} for the harmonic frequency of the mode in question. We attribute the enormous discrepancy between this value and the 18i cm^{-1} obtained from MP2/6-31+G* to the high degree of anharmonicity in the vibrational mode

TABLE 12: MP2/6-31+G* Single Points for $O_2CCH_2CO_2^-$ Displaced from Its Optimized C_2 Geometry by a Scalar Multiple λ of Its Lowest-Frequency Normal Mode Eigenvector[a]

λ 10^{-3} Å	max atomic displacement, Å	$E(\lambda) - E(0)$, eV
1.923 08	0.001	0.000 021 5
−1.923 08	0.001	0.000 022 7
5.769 23	0.003	0.000 194 0
−5.769 23	0.003	0.000 191 4
9.615 38	0.005	0.000 544 2
−9.615 38	0.005	0.000 981 1
13.461 54	0.007	0.001 047 7
−13.461 54	0.007	0.001 043 4
17.307 69	0.009	0.970 489 4
−17.307 69	0.009	0.985 112 7
19.230 77	0.010	0.969 759 0
−19.230 77	0.010	0.972 387 3

[a] $\lambda = 0$ is the C_2 conformation.

(anharmonicity that is hardly surprising in light of the low frequency).

Augmenting our basis to 6-311++G** produces essentially the same four optimized structures for $O_2CCH_2CO_2^-$ and the same ordering of their relative energies. With a basis of this size we are unable to calculate MP2 frequencies; nevertheless, a preponderance of evidence supports our identification of a C_2 local minimum on the monoanion potential surface.

Detachment Energies. Asessment of a detachment energy for malonate is complicated by the buckling of the potential surface that occurs upon electron detachment from $O_2CCH_2CO_2^{2-}$. In at least one dimension, the dianion exhibits an exceedingly flat potential surface and thus has multiple accessible conformers which may or may not be isoenergetic on the *mono*anion surface. Hence vertical electron detachment from C_2(keto) $O_2CCH_2CO_2^{2-}$ may be a far different process than vertical detachment from the energetically equivalent C_s(keto) conformer. In either case, vertical electron detachment produces a monoanion far from the global minimum on the potential surface, since the enol isomer of $O_2CCH_2CO_2^-$ is more stable than the keto isomer. We therefore report P3 and ΔMP2 VEDEs from both the C_2 and C_s conformers of keto $O_2CCH_2CO_2^{2-}$ and list these in Table 13. For completeness, we also include a few VEDEs from the less stable enol isomer of $O_2CCH_2CO_2^{2-}$; this species is clearly unbound even in the vertical sense.

In calculating an adiabatic detachment energy, it matters little whether one uses the C_2(keto) or the C_s(keto) geometry of the dianion, since the energy difference between the two is essentially zero. In Table 14, we tabulate AEDEs and relative conformational energies obtained at the MP2 level with several large basis sets.

The ΔMP2 VEDEs of the two keto conformers differ in sign and indicate that C_s(keto) $O_2CCH_2CO_2^{2-}$ is bound but the C_2-(keto) conformer is not. The disparity arises due to fundamental differences in the structure of the HOMO of each conformer. In C_2(keto) malonate, the HOMO of both anions is highly delocalized (Figure 5), while for the C_s (keto) anions the HOMO is localized almost entirely on one carboxylate group, as shown in Figure 6. Note from Table 13, however, that many of our ΔMP2 vertical detachment calculations for the C_2(keto) geometry suffer from spin contamination, with $\langle S^2\rangle_{UHF}$ for the (unrestricted) HF reference function of the monoanion as large as 0.89 in some cases. This does not bode well for the reliability of these VEDEs.

The P3 VEDEs of Table 13 are more reliable and in each case give the same detachment energy for both keto conformers.

TABLE 13: P3 and ΔMP2 Vertical Detachment Energies for $O_2CCH_2CO_2^{2-}$ [a]

		VEDE, eV	
basis set	structure	ΔMP2	P3
MP2/6-31+G* Geometry			
6-31+G*	C_s(keto)	0.34	−0.10
	C_2(keto)	−0.29[b]	−0.10
	C_s(enol)	−1.74[b]	−0.43
			−1.88
6-311++G**	C_s(keto)	0.31	0.01
	C_2(keto)	−0.23	0.01
	C_s(enol)	−1.65[b]	−0.30
			−1.76
6-311++G(2df,p)	C_s(keto)	0.50	0.18
	C_2(keto)	−0.14[b]	0.18
	C_s(enol)	−1.52[b]	
6-311+++G**	C_s(keto)	0.31	0.04
	C_2(keto)	−0.24	0.04
	C_s(enol)	−1.64[b]	−0.25
			−1.73
MP2/6-311++G** Geometry			
6-311++G**	C_s(keto)	0.29	−0.05
	C_2(keto)	−0.36[b]	−0.05
	C_s(enol)	−1.79[b]	−0.31
			−1.85
6-311++(2df,p)	C_s(keto)	0.48	0.12
	C_2(keto)	−0.19[b]	0.12
	C_s(enol)	−1.66[b]	
6-311++G(2df,2pd)	C_s(keto)		0.12
	C_2(keto)		0.12
	C_s(enol)	−1.65[b]	
6-311++G(3d2f,2pd)	C_s(keto)		0.17
	C_2(keto)		0.17
6-311+++G**	C_s(keto)	0.30	−0.02
	C_2(keto)	−0.35[b]	−0.02
	C_s(enol)	−1.78[b]	−0.26
			−1.82
6-311+++G(2df,p)	C_s(keto)		0.16
	C_2(keto)		0.16
	C_s(enol)		
6-311+++G(2df,2pd)	C_s(keto)		0.16
	C_2(keto)		0.16
	C_s(enol)		

[a] ΔMP2 detachment energies correspond to removal of an electron from the HOMO, which has a' symmetry for the C_s (keto) structure, b symmetry for the C_2(keto) structure, and a'' symmetry for the C_s(enol) structure. P3 calculations for the keto structures correspond in each case to the HOMO, while for the enol isomer the first P3 detachment energy listed is for the a' HOMO − 1 and the second is for the HOMO. The "+ + +" bases contain extra diffuse functions on the heavy atoms. [b] $0.84 \le \langle S^2\rangle_{UHF} \le 0.89$ before annihilation for these (nonoptimized) structures of $O_2CCH_2CO_2^-$.

These calculations also demonstrate that the enol isomer of the dianion is highly unstable with respect to vertical electron detachment. For the keto structures, however, the detachment energy is quite close to zero and in fact its sign depends on the basis set. When only one set of heavy-atom polarization functions is included (6-31+G*, 6-311++G**, and 6-311+++G**), we obtain small but negative detachment energies. Additional polarization functions on the light atoms appear to matter little, but additional polarization functions on the heavy atoms produce a VEDE as large as +0.17 eV (3.9 kcal/mol) for both conformers. This indicates that the dianion may be vertically bound-albeit by only a few kcal/mol−and might be detected as a metastable species in a careful experiment. Wang et al.[5] report no such observation in their studies of dicarboxylates; however, these authors are limited by their detection scheme to lifetimes greater than 0.1 s.

Succinate. Structures of $O_2C(CH_2)_2CO_2^{2-}$ and $O_2C(CH_2)_2CO_2^-$. We find the succinate anions to be structurally

TABLE 14: ΔMP2 Adiabatic Detachment Energies for $O_2CCH_2CO_2^{2-}$ [a]

basis set	energy[b] dianion	energy[b] monoanion	AEDE, eV
	MP2/6-31+G* Geometry		
6-31+G*	−415.347 63 [C_s(keto)]	−415.405 00 [C_s(enol)]	−1.56[c]
	0.002 [C_2(keto)]	0.71 [C_2(keto)]	
	0.63 [C_s(enol)]	1.34 [C_1(keto)]	
		1.52 [C_s(keto)]	
6-311++G**	−415.644 35 [C_2(keto)]	−415.708 24 [C_s(enol)]	−1.74
	0.00 [C_s(keto)]	0.80 [C_2(keto)]	
	0.46 [C_s(enol)]	1.47 [C_1(keto)]	
		1.65 [C_s(keto)]	
6-311+++G**	−415.675 64 [C_2(keto)]	−415.736 06 [C_s(enol)]	−1.64
	0.00 [C_s(keto)]	0.71 [C_2(keto)]	
	0.54 [C_s(enol)]	1.38 [C_1(keto)]	
		1.56 [C_s(keto)]	
6-311++G(2df,p)	−415.878 17 [C_2(keto)]	−415.940 21 [C_s(enol)]	−1.69
	0.00 [C_s(keto)]	0.88 [C_2(keto)]	
	0.37 [C_s(enol)]	1.59 [C_1(keto)]	
		1.77 [C_s(keto)]	
6-311++G(2df,2pd)	−415.885 83 [C_s(keto)]	−415.949 74 [C_s(enol)]	−1.74
	0.00 [C_2(keto)]	0.94 [C_2(keto)]	
	0.30 [C_s(enol)]	1.65 [C_1(keto)]	
		1.83 [C_s(keto)]	
	MP2/6-311++G** Geometry		
6-311++G**	−415.644 82 [C_2(keto)]	−415.709 37 [C_s(enol)]	−1.76
	0.00 [C_s(keto)]	0.81 [C_2(keto)]	
	0.45 [C_s(enol)]	1.48 [C_1(keto)]	
		1.66 [C_s(keto)]	
6-311+++G**	−415.673 64 [C_2(keto)]	−415.737 20 [C_s(enol)]	−1.73
	0.00 [C_s(keto)]	0.79 [C_2(keto)]	
	0.46 [C_s(enol)]	1.40 [C_1(keto)]	
		1.64 [C_s(keto)]	
6-311++G(2df,p)	−415.878 97 [C_2(keto)]	−415.941 63 [C_s(enol)]	−1.71
	0.00 [C_s(keto)]	0.90 [C_2(keto)]	
	0.36 [C_s(enol)]	1.61 [C_1(keto)]	
		1.79 [C_s(keto)]	
6-311++G(2df,2pd)	−415.886 63 [C_s(keto)]	−415.951 23 [C_s(enol)]	−1.76
	0.00 [C_2(keto)]	0.96 [C_2(keto)]	
	0.29 [C_s(enol)]	1.67 [C_1(keto)]	
		1.85 [C_s(keto)]	

[a] Optimizations were performed with two different basis sets, then single point energies were calculated at these geometries using larger basis sets. The "+ + +" bases contain additional diffuse functions on the heavy atoms. [b] Minimum-energy conformer is listed in hartrees; relative energies of the remaining conformers are given in electronvolts. [c] At this level of theory, calculated harmonic frequencies give $AEDE_0 = -0.86$ eV.

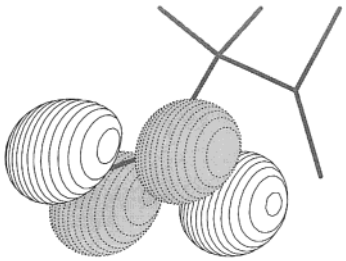

Figure 6. Highest occupied molecular orbital of $^2A'$ $O_2CCH_2CO_2^-$, as obtained at the MP2/6-311++G** geometry. The dianion's HOMO includes some contribution from orbitals on both carboxylate groups but is still highly localized on one end of the molecule.

quite similar to their malonate homologues. The major difference between the two species is the near stability of the succinate dianion, while $O_2CCH_2CO_2^{2-}$ is clearly unstable. We attribute this distinction to the high degree of localization exhibited by the succinate dianion's HOMO, which keeps the electrons in that orbital on one carboxylate group and well separated from the other negatively charged carboxylate group.

Our lowest energy MP2 structure for $O_2C(CH_2)_2CO_2^{2-}$ (optimized using either the 6-31+G* or 6-311++G** basis) exhibits C_2 symmetry, as shown in Figure 7a, and is highly reminiscent of our minimum-energy structure for $O_2CCH_2CO_2^{2-}$.

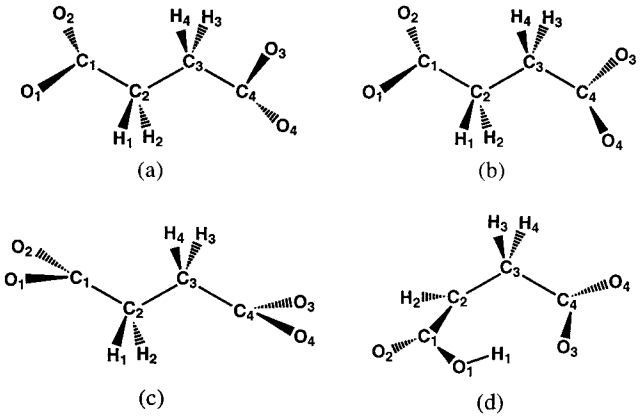

Figure 7. MP2-optimized structures for succinate anions. (a) C_2(keto) potential minimum of $O_2C(CH_2)_2CO_2^{2-}$; (b) C_i(keto) transition state of $O_2C(CH_2)_2CO_2^{2-}$; (c) C_2 and C_i keto structures of $O_2C(CH_2)_2CO_2^-$; (d) C_1 (enol) structure of $O_2C(CH_2)_2CO_2^-$ and $O_2C(CH_2)_2CO_2^{2-}$.

One O−C−C−H dihedral angle on each carboxylate moiety is only 7° from planarity with an O−H distance of 2.478 Å. The remaining C−O bond of each CO_2 group nearly aligns with a C−H bond of the far methylene group. The O−H interactions are not strong, and rotation of one CO_2 moiety produces a

TABLE 15: Energies of Optimized Succinate Structures

basis set	structure	*E*	low freq., cm^{-1}
$O_2C(CH_2)_2CO_2^{2-}$			
6-31+G*	C_2(keto)	−454.544 26[a]	31.6(*A*)
	C_i(keto)	0.03[b]	23.5*i*(A_u)
	C_1(enol)	1.53[b]	66.9(*A*)
6-311++G**	C_2(keto)	−454.884 26[a]	
	C_i(keto)	0.03[b]	
	C_1(enol)	1.35[b]	
$O_2C(CH_2)_2CO_2^-$			
6-31+G*	C_1(enol)	−454.576 05[a]	
	C_2(keto)	0.50[b]	
	C_i(keto)	0.50[b]	
6-311++G**	C_1(enol)	−454.922 48[a]	
	C_i(keto)	0.61[b]	
	C_2(keto)	0.61[b]	

[a] MP2 energy in atomic units. [b] Energy (eV) relative to the lowest-energy structure at the same level of theory.

TABLE 16: MP2-Optimized Bond Lengths for the Keto Isomer of Succinate[a]

basis set	point group	bond lengths, Å				
		C_1-O_1	C_1-O_2	C_1-C_2	C_2-C_3	O_1-H_1
$O_2C(CH_2)_2CO_2^{2-}$						
6-31+G*	C_2	1.280	1.274	1.548	1.530	2.475
	C_i	1.279	1.276	1.548	1.535	2.494
6-311++G**	C_2	1.269	1.265	1.552	1.531	2.478
	C_i	1.268	1.266	1.552	1.536	2.499
$O_2C(CH_2)_2CO_2^-$						
6-31+G*	C_2	1.249	1.249	1.651	1.481	2.497
	C_i	1.249	1.249	1.651	1.481	2.497
6-311++G**	C_2	1.236	1.236	1.669	1.478	2.494
	C_i	1.237	1.237	1.667	1.478	2.496

[a] Atom labels refer to Figure 7.

transition state of C_i symmetry that is only 0.7 kcal/mol higher in energy. The vibrational mode that interconverts the two has a frequency of 31.6 cm^{-1} in the C_2 conformer (making it the lowest energy mode) and maps to an imaginary frequency of 23.5*i* cm^{-1} in the transition state. Like those of malonate, the carboxylate groups of the succinate dianion behave as free rotors (Tables 15−17).

These results are in good agreement with optimized keto structures obtained recently by Skurski et al.[19] using MP2 optimization and Dunning's aug-cc-pVDZ+2s2p basis.[26] These authors obtain C_{2h} minima for both mono- and dianion; however, facile rotation of the carboxylate groups lowers the symmetry to either C_2 or C_i, as in our results. Other bond angles as well as bond lengths calculated by Skurski et al. are in good agreement with the present work.

In addition to the keto structures, we also optimize the enol isomer to obtain the structure shown in Figure 7d, in which the carbon backbone is bent out of the plane to facilitate a H_1-O_3 hydrogen bond. Despite this feature, the enol isomer is far higher in energy than the keto isomer. Optimized geometry data for the enol isomer are listed in Tables 18 and 19.

For $O_2C(CH_2)_2CO_2^-$, our lowest-energy, optimized structure is an enol isomer similar to that of the dianion, while C_2 and C_i keto structures (Figure 7c) lie approximately 0.6 eV (14 kcal/mol) higher in energy. The C_2 and C_i conformers of the keto isomer are essentially the same, both energetically and structurally, and we consider the difference numerical rather than physical in origin. The *a* HOMO of the C_2 conformer is shown in Figure 8. The C_i structure has essentially the same HOMO, which is also totally symmetric (a_g).

Detachment Energies. In Table 20, we list ΔMP2 AEDEs obtained using several large basis sets. For the largest of these we are unable to calculate the energy of the enol structure, which lacks any symmetry, and consequently we do not list AEDEs in these cases. The calculated detachment energies indicate an electron that is unbound by about 1.0 eV (23 kcal/mol). Additional diffuse functions do not change the detachment energy but polarization functions do have a noticeable effect, driving the AEDE toward zero as more functions are added. It is noteworthy that for each single-point basis set the two levels of optimization (MP2/6-31+G* versus MP2/6-311++G**) produce AEDEs that are the same to within 0.02 eV, suggesting that in future studies of larger dicarboxylates one may omit the more difficult optimization.

Table 21 presents ΔMP2 and P3 VEDEs for succinate. As with malonate, the ΔMP2 results are highly suspect due to spin contamination in the single-point calculation of the monoanion at the dianion's optimized geometry. Nevertheless, every calculated VEDE for keto succinate is positive, indicating a (vertically) bound electron. Our best P3 calculation places this vertical detachment barrier at 0.6 eV (15 kcal/mol). On the other hand, the enol isomer of the dianion is clearly unstable with respect to electron detachment, just as in malonate. (In fact, the dianion HOMO has a positive SCF eigenvalue, indicating that even in the frozen-orbital, Koopmans's theorem picture, the enol isomer of $O_2C(CH_2)_2CO_2^{2-}$ contains an unbound electron.)

Using the ΔCCSD(T) method, Skurski et al.[19] report a VEDE of 0.39 eV for succinate, which is roughly comparable to our ΔMP2 values but substantially lower than our P3 estimates of the detachment energy.

Conclusions

We have investigated the properties of the first three homologues in the $O_2C(CH_2)_nCO_2$ sequence, presenting MP2/6-31+G*- and MP2/6-311++G**-optimized structures for oxalate, malonate, and succinate mono- and dianions, along with adiabatic and vertical electron detachment energies from the

TABLE 17: MP2-Optimized Bond Angles for the Keto Isomer of Succinate[a]

basis set	point group	angles, deg			
		$O_1-C_1-O_2$	$C_1-C_2-C_3$	$O_1-C_1-C_2-H_1$	$O_2-C_1-C_3-H_3$
$O_2C(CH_2)_2CO_2^{2-}$					
6-31+G*	C_2	126.48	114.86	11.25	10.95
	C_i	126.54	113.65	4.13	0.40
6-311++G**	C_2	127.02	114.69	7.24	9.09
	C_i	127.08	113.51	8.04	3.45
$O_2C(CH_2)_2CO_2^-$					
6-31+G*	C_2	135.52	107.61	30.52	21.11
	C_i	135.52	107.60	30.68	21.23
6-311++G**	C_2	136.62	107.63	30.26	21.32
	C_i	136.63	107.59	30.55	21.56

[a] Atom labels refer to Figure 7.

TABLE 18: MP2-Optimized Bond Lengths (Å) for the Enol Isomer of Succinate[a]

	dianion		monoanion	
bond	6-31+G*	6-311++G**	6-31+G*	6-311++G**
O_1-H_1	1.000	0.989	1.053	1.066
C_1-O_1	1.414	1.407	1.330	1.319
C_1-O_2	1.278	1.266	1.236	1.229
C_1-C_2	1.395	1.397	1.477	1.481
C_2-H_2	1.090	1.088	1.085	1.084
C_2-C_3	1.515	1.516	1.487	1.488
C_3-C_4	1.546	1.550	1.566	1.567
C_4-O_4	1.274	1.264	1.249	1.236
C_4-O_3	1.284	1.275	1.286	1.280
O_3-H_1	1.776	1.746	1.493	1.397

[a] Atom labels refer to Figure 7d.

TABLE 19: MP2-Optimized Bond Angles (deg) for the Enol Isomer of Succinate[a]

	dianion		monoanion	
angle	6-31+G*	6-311++G**	6-31+G*	6-311++G**
$O_1-C_1-O_2$	115.3	115.7	122.4	123.4
$C_1-O_1-H_1$	107.0	106.5	109.5	109.2
$O_1-C_1-C_2$	116.0	115.7	116.4	115.9
$C_1-C_2-C_3$	125.1	125.0	124.1	123.5
$C_2-C_3-C_4$	118.2	117.7	114.0	113.5
$C_3-C_4-O_3$	115.5	115.1	114.4	114.0
$C_3-C_4-O_4$	118.4	118.5	128.0	117.8
$C_4-O_3-H_1$	104.5	104.8	111.0	111.0
$O_2-C_1-C_2-H_2$	0.5	1.5	21.2	19.9
$H_4-C_3-C_4-O_4$	2.4	3.4	4.3	3.5
$C_1-C_2-C_4-O_3$	5.3	3.7	10.4	8.9

[a] Atom labels refer to Figure 7d.

dianion. Optimized D_{2d} and D_{2h} structures obtained for oxalate concur with previous results obtained at lower levels of theory.

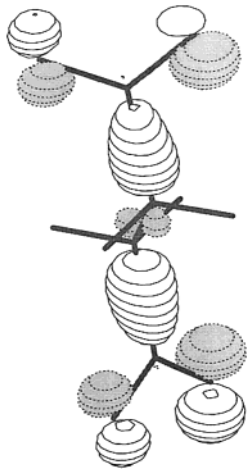

Figure 8. Highest occupied molecular orbital of ^1A $O_2C(CH_2)_2CO_2^{2-}$, as obtained at the MP2/6-311++G** geometry. The a_g HOMO of the C_i conformer is qualitatively indistinguishable.

Calculated detachment energies imply that $C_2O_4^{2-}$ is unbound, both vertically and adiabatically.

For the malonate and succinate dianions we find both keto and enol isomers. The keto structure is the more stable isomer for both dianions and is characterized by carboxylate groups that rotate freely. For both monoanions the enol isomer is lower in energy, and this structure is much more rigid owing to intramolecular hydrogen bonding. Both the malonate and succinate dianions are thermodynamically unstable with respect to electron detachment.

Vertical detachment energies obtained from single-point calculations of the monoanion's energy at the dianion's minimum-energy geometry are unreliable for malonate and succinate

TABLE 20: ΔMP2 Adiabatic Detachment Energies for $O_2C(CH_2)_2CO_2^{2-}$

	energy[a]		
basis set	dianion	monoanion	AEDE, eV
	MP2 6-31+G* Geometry		
6-31+G*	−454.544 26 [C_2(keto)]	−454.576 05 [C_1(enol)]	−0.87
	0.03 [C_i(keto)]	0.50 [C_2(keto)]	
	1.53 [C_1(enol)]	0.50 [C_i(keto)]	
6-311+G**	−454.883 03 [C_2(keto)]	−454.920 91 [C_1(enol)]	−1.03
	0.03 [C_i(keto)]	0.60 [C_i(keto)]	
	1.33 [C_1(enol)]	0.60 [C_2(keto)]	
6-311++G**	−454.883 74 [C_2(keto)]	−454.921 46 [C_1(enol)]	−1.03
	0.03 [C_i(keto)]	0.60 [C_i(keto)]	
	1.33 [C_1(enol)]	0.60 [C_2(keto)]	
6-311+G(2df,p)	−455.137 45 [C_2(keto)]	−455.172 52 [C_1(enol)]	−0.95
	0.03 [C_i(keto)]	0.64 [C_i(keto)]	
	1.32 [C_1(enol)]	0.64 [C_2(keto)]	
6-311++G(2df,p)	−455.137 90 [C_2(keto)]	−455.172 93 [C_1(enol)]	−0.95
	0.03 [C_i(keto)]	0.65 [C_i(keto)]	
	1.31 [C_1(enol)]	0.65 [C_2(keto)]	
6-311++G(2df,2pd)[b]	−455.152 79 [C_2(keto)]	−455.163 70 [C_2(keto)]	
	0.03 [C_i(keto)]	0.00 [C_i(keto)]	
6-311+++G(2df,2pd)[b,c]	−455.178 51 [C_2(keto)]	−455.189 20 [C_i(keto)]	
	0.03 [C_i(keto)]	0.00 [C_2(keto)]	
	MP2 6-311++G** Geometry		
6-311++G**	−454.884 26 [C_2(keto)]	−454.922 48 [C_1(enol)]	−1.04
	0.03 [C_i(keto)]	0.61 [C_i(keto)]	
	1.34 [C_1(enol)]	0.61 [C_2(keto)]	
6-311++G(2df,p)	−455.138 70 [C_2(keto)]	−455.174 33 [C_1(enol)]	−0.97
	0.03 [C_i(keto)]	0.65 [C_2(keto)]	
	1.31 [C_1(enol)]	0.65 [C_i(keto)]	
6-311++G(2df,2pd)[b]	−455.153 61 [C_2(keto)]	−455.164 84 [C_2(keto)]	
	0.03 [C_i(keto)]	0.00 [C_i(keto)]	

[a] Minimum-energy conformer is listed in hartrees; relative energies of the remaining conformers are given in electronvolts. [b] We are unable to calculate the energy of the enol isomer using these large basis sets so no AEDE is listed. [c] Includes additional diffuse functions on the heavy atoms.

TABLE 21: ΔMP2 and P3 Vertical Detachment Energies for MP2-Optimized $O_2C(CH_2)_2CO_2^{2-}$ [a]

		VEDE, eV	
basis set	structure	ΔMP2	P3
MP2 6-31+G* Geometry			
6-31+G*	C_2(keto)	0.33	0.57
	C_i(keto)	0.39	0.53
	C_1(enol)	−1.28	−1.96
6-311++G**	C_2(keto)	0.33	0.67
	C_i(keto)	0.39	0.63
	C_1(enol)	−1.64	−1.84
6-311++G(2df,p)	C_2(keto)	0.50	
	C_i(keto)	0.55	
	C_1(enol)	−1.53	
MP2 6-311++G** Geometry			
6-311++G**	C_2(keto)	0.28	0.60
	C_i(keto)	0.33	0.56
	C_1(enol)	−1.78	−1.93
6-311++G(2df,p)	C_2(keto)	0.44	
	C_i(keto)	0.49	
	C_1(enol)	−1.66	

[a] C_i detachment energies correspond to the a_g HOMO and C_2 energies to the a HOMO. Each MP2 single-point for the monoanion at the dianion geometry had $0.83 \leq \langle S^2 \rangle_{UHF} \leq 0.88$ before annihilation.

because they suffer from serious spin contamination; we instead rely on P3 vertical detachment energies. These calculations indicate a small (<0.2 eV) vertical detachment barrier in the malonate dianion, but for succinate, our calculated barrier to vertical detachment is 0.6 eV. This supports the hypothesis that $O_2C(CH_2)_2CO_2^{2-}$ may account for a weak mass spectrum signal at $m/z = 58$ that has been reported by several groups.[4,6]

In future work, we would like to investigate other dicarboxylate species that lie on the "cusp" of stability, including glutarate $[O_2C(CH_2)_3CO_2]$ and the succinate−water complex $O_2C(CH_2)_2CO_2^{2-}\cdot H_2O$, both of which have been detected experimentally.

Acknowledgment. O. Dolgounitcheva and V. G. Zakrzewski provided extensive technical advice and support for this work. Acknowledgment is made to the donors of the Petroleum Research Fund, administered by the American Chemical Society, for partial support of this research. This work also was supported by the National Science Foundation under grant CHE-9873897 and by Gaussian, Incorporated.

References and Notes

(1) Simons, J.; Jordan, K. D. *Chem. Rev.* **1987**, *87*, 535. Kalcher, J.; Sax, A. F. *Chem. Rev.* **1994**, *94*, 2291. Scheller, M. K.; Compton, R. N.; Cederbaum, L. S. *Science* **1995**, *270*, 1160. Freeman, G. R.; March, N. H. *J. Phys. Chem.* **1996**, *100*, 4331 and references therein.

(2) Boldyrev, A. I.; Gutowski, M.; Simons, J. *Acc. Chem. Res.* **1996**, *29*, 497.

(3) Ding, C.-F.; Wang, X.-B.; Wang, L.-S. *J. Chem. Phys.* **1999**, *110*, 3635. Wang, X.-B.; Wang, L.-S. *Phys. Rev. Lett.* **1999**, *83*, 3402. Wang, X.-B.; Ferris, K.; Wang, L.-S. *J. Phys. Chem. A* **2000**, *104*, 25.

(4) Maas, W. P. M.; Nibbering, N. M. M. *Int. J. Mass Spectrom. Ion Proc.* **1989**, *88*, 257.

(5) Wang, L. S.; Ding, C.-F.; Wang, X.-B.; Nicholas, J. B. *Phys. Rev. Lett.* **1998**, *81*, 2667.

(6) Ding, C.-F.; Wang, X.-B.; Wang, L.-S. *J. Phys. Chem. A* **1998**, *102*, 8633.

(7) Wang, X.-B.; Ding, C.-F.; Wang, L.-S. *Phys. Rev. Lett.* **1998**, *81*, 3351. Wang, L.-S.; Ding, C.-F.; Wang, X.-B. *Rev. Sci. Instrum.* **1999**, *70*, 1957. Wang, L.-S.; Wang, X.-B. *J. Phys. Chem. A* **2000**, *104*, 1978.

(8) Aplin, R. T.; Moloney, M. G.; Newby, R.; Wright, E. *J. Mass Spectrom.* **1999**, *34*, 60.

(9) Although Maas and Nibbering (ref 4) do observe a weak signal in the mass spectrum at an m/z ratio corresponding to $O_2C(CH_2)_2CO_2^{2-}$, for this particular species they are unable to distinguish this dianion from the singly charged distonic radical anion $\cdot CHCO_2^-$.

(10) Fleischman, S. H.; Jordan, K. D. *J. Phys. Chem.* **1987**, *91*, 1300.

(11) Rossi, A. R.; Jordan, K. D. *J. Chem. Phys.* **1979**, *70*, 4422. Yoshioka, Y.; Jordan, K. D. *J. Am. Chem. Soc.* **1980**, *102*, 2621.

(12) Radom, L. In *Modern Theoretical Chemistry*; Schaefer, H. F., Ed.; Plenum: New York, 1977; Vol. 4. Radom, L. *Aust. J. Chem.* **1979**, *29*, 1635.

(13) Clark, T.; Schleyer, P. v. R. *J. Comput. Chem.* **1981**, *2*, 20.

(14) Dewar, M. J. S.; Zheng, Y.-J. *J. Mol. Struct. (THEOCHEM)* **1990**, *209*, 157.

(15) Gottschalk, K. E.; Hiskey, R. G.; Pedersen, L. G.; Koehler, K. A. *J. Mol. Struct. (THEOCHEM)* **1981**, *76*, 197.

(16) Briggman, B.; Oskarsson, A. *Acta Crystallogr. B* **1977**, *33*, 1900.

(17) Han, S. J.; Kim, Y. J.; Kang, Y. K. *J. Mol. Struct. (THEOCHEM)* **1996**, *369*, 145.

(18) Deerfield, D. W.; Pedersen, L. G. *J. Mol. Struct. (THEOCHEM)* **1996**, *368*, 163.

(19) Skurski, P.; Simons, J.; Wang, X.-B.; Wang, L.-S. *J. Am. Chem. Soc.* **2000**, *112*, 4499.

(20) Frisch, M. J.; Trucks, G. W.; Schlegel, H. B.; Scuseria, G. E.; Robb, M. A.; Cheeseman, J. R.; Zakrezewski, V. G.; Montgomery, J. A.; Stratmann, R. E.; Burant, J C.; Dapprich, S.; Millam, J. M.; Daniels, A. D.; Kudin, K. N.; Strain, M. C.; Farkas, O.; Tomasi, J.; Barone, V.; Cossi, M.; Cammi, R.; Mennucci, B.; Pomelli, C.; Adamo, C.; Clifford, S.; Ochterski, J.; Peterson, G. A.; Ayala, P. Y.; Cui, Q.; Morokuma, K.; Malick, D. K.; Rabuck, A. D.; Raghavachari, K.; Foresman, J. B.; Cioslowski, J.; Ortiz, J. V.; Baboul, A. G.; Stefanov, B. B.; Liu, G.; Liashenko, A.; Piskorz, P.; Komaromi, I.; Gomperts, R.; Martin, R. L.; Fox, D. J.; Keith, T.; Al-Laham, M. A.; Peng, C. Y.; Nanayakkara, A.; Gonzalez, C.; Challacombe, M.; Gill, P. M. W.; Johnson, B.; Chen, W.; Wong, M. W.; Andres, J. L.; Gonzalez, C.; Head-Gordon, M.; Replogle, E. S.; Pople, J. A. *Gaussian 98*, Revision A.7; Gaussian, Inc.: Pittsburgh, PA, 1998.

(21) Møller, C.; Plesset, M. S. *Phys. Rev.* **1934**, *46*, 618. Binkley, J. S.; Pople, J. A. *Int. J. Quantum Chem.* **1975**, *9*, 229. Binkley, J. S.; Seeger, R. *Int. J. Quantum Chem.* **1976**, *10*, 1. Bartlett, R. J. *Annu. Rev. Phys. Chem.* **1981**, *32*, 359.

(22) Hehre, W. J.; Ditchfield, R.; Pople, J. A. *J. Chem. Phys.* **1972**, *56*, 2257. McLean, A. D.; Chandler, G. S. *J. Chem. Phys.* **1980**, *72*, 5639. Clark, T.; Chandrasekhar, J.; Spitznagel, G. W.; Schleyer, P. v. R. *J. Comput. Chem.* **1983**, *4*, 294.

(23) Linderberg, J.; Öhrn, Y. *Propagators in Quantum Chemistry*; Academic Press: New York, 1973. Ortiz, J. V. *Adv. Quantum Chem.* **1999**, *35*, 33.

(24) Ortiz, J. V. *J. Chem. Phys.* **1996**, *104*, 7599. Ortiz, J. V.; Zakrzewski, V. G. *J. Chem. Phys.* **1996**, *105*, 2762.

(25) Hariharan, P. C.; Pople, J. A. *Theor. Chim. Acta*, **1973**, *28*, 213. Krishnan, R.; Binkley, J. S.; Seeger, R.; Pople, J. A. *J. Chem. Phys.* **1980**, *72*, 650. Frisch, M. J.; Pople, J. A.; Binkley, J. S. *J. Chem. Phys.* **1984**, *80*, 3265.

(26) Kendall, R. A.; Dunning, T. H.; Harrison, R. J. *J. Chem. Phys.* **1992**, *96*, 6796.